Scanning tunneling microscopy images of a triangular quantum dot of InAs

2008 J. Phys.: Condens. Matter 20 285220

(http://iopscience.iop.org/0953-8984/20/28/285220)

IOP PUBLISHING JOURNAL OF PHYSICS: CONDENSED MATTER

J. Phys.: Condens. Matter **20** (2008) 285220 (6pp) doi:10.1088/0953-8984/20/28/285220

Scanning tunneling microscopy images of a triangular quantum dot of InAs

Takuya Kumagai and Akira Tamura[1]

Faculty of Materials Sciences, Graduate School, Saitama Institute of Technology, 1690 Fusaiji, Fukaya-City, 369-0293 Saitama, Japan

Received 17 December 2007, in final form 28 April 2008
Published 24 June 2008
Online at stacks.iop.org/JPhysCM/20/285220

Abstract

On the basis of a simple one-particle model we derived eigenstates and eigenenergies of electrons confined in an equilateral triangular quantum dot of InAs (111)A surface. Considering two subbands formed by the band bending in the InAs surface, we explained STM images observed in the differential conductance mode. It is pointed out that contributions from two subbands are indispensable for analyzing the STM images on the InAs quantum dot. Moreover, it is shown that reduction in the subband energy level induced by an applied bias voltage plays an important role in obtaining proper STM images.

1. Introduction

Quantum corrals (QC) observed by STM (scanning tunneling microscope) reveal the wave feature of electrons on surfaces. Since Crommie *et al* [1] fabricated a circular QC for the first time, many kinds of QCs have been intensively studied; linear, rectangular, triangular, elliptical and hexagonal QCs on noble metal surfaces [2, 3] and Co islands [4]. The electrons confined in such QCs originate from the Shockley electrons which exist in the plane parallel to the surface and have decaying tails on both sides the surface [5]. Previously [6] we calculated electron states confined in a triangular quantum corral and obtained the differential conductance ($\mathrm{d}I/\mathrm{d}V$) images for Ag QCs on Ag(111) surface. Our images are consistent with the experimental ones observed by Rieder *et al* [7]. As regards nanostructures on semiconductor surfaces, many kinds of research have been carried out [8]. Among them Kanisawa *et al* [9, 10] observed STM images of an InAs quantum dot (QD) in the differential conductance ($\mathrm{d}I/\mathrm{d}V$) mode. In the case of the InAs QD, there exist subbands [9, 10] caused by the band bending just inside the surface, which is different from the single band associated with the Shockley state on noble metal surfaces. The electrons occupying each subband form a two-dimensional electron gas (2DEG) in the direction parallel to the surface. In the direction normal to the surface, the electrons have decaying tails into the bulk. Kanisawa *et al* [10] claimed that the $\mathrm{d}I/\mathrm{d}V$ is proportional to the local density of states (LDOS) of the confined 2DEG. Here, we derive $\mathrm{d}I/\mathrm{d}V$ images by using our expression for the $\mathrm{d}I/\mathrm{d}V$ [6] and clarify the main factors which form STM images. We also compare our $\mathrm{d}I/\mathrm{d}V$ images with LDOS images calculated by Kanisawa *et al* [10].

[1] Author to whom any correspondence should be addressed.

2. Eigenstates of electrons confined in an equilateral triangular QD

On the basis of a one-particle model we consider the electron confined in an equilateral triangle of an InAs QD. We treat three edges surrounding the QD as potential barriers that confine 2DEG. Here, we assume that the height is infinite. Considering the effect of the band bending near the surface of InAs, we solve a one-particle Schrödinger equation for the potential including the z-component;

$$-\frac{\hbar^2}{2m^*}\nabla^2\Psi(\boldsymbol{r}) + [V(\boldsymbol{\rho}) + V_\perp(z)]\Psi(\boldsymbol{r}) = E_{3\mathrm{D}}\Psi(\boldsymbol{r}), \quad (1)$$

where $\boldsymbol{r}$ represents a position vector of an electron and is defined as $\boldsymbol{r} = (\boldsymbol{\rho}, z)$ with a two-dimensional vector $\boldsymbol{\rho} = (x, y)$ on the QD surface. m^* is the effective mass of the electron. The two-dimensional potential $V(\boldsymbol{\rho})$ confines 2DEG formed on the surface of the InAs QD. Another potential $V_\perp(z)$ represents an attractive potential coming from band bending under the surface, which yields several bound states (subband states) labeled j. With a separation of variables method; $\Psi(\boldsymbol{r}) = \psi(\boldsymbol{\rho})\phi_j(z)$, we have

$$-\frac{\hbar^2}{2m^*}\left(\frac{\partial^2}{\partial x^2} + \frac{\partial^2}{\partial y^2}\right)\psi(\boldsymbol{\rho}) + V(\boldsymbol{\rho})\psi(\boldsymbol{\rho}) = E\psi(\boldsymbol{\rho}), \quad (2)$$

and

$$-\frac{\hbar^2}{2m^*}\frac{\mathrm{d}^2}{\mathrm{d}z^2}\phi_j(z) + V_\perp(z)\phi_j(z) = E_{zj}\phi_j(z), \quad (3)$$

where we set the bottom of the potential $V(\boldsymbol{\rho})$ at E_{zj}. The value $E + E_{zj}$ corresponds to the energy level of the confined electron. To derive the eigenstates $\psi(\boldsymbol{\rho})$ and the eigenenergies E, we considered the process [6] that an electron inside the QD proceeds to a barrier wall, collides with the wall, experiences subsequent reflections at other walls and the electron finally returns to the initial point. In the previous article [6], we derived the eigenstates and the eigenenergies of the electron confined in the equilateral triangular QC. The characteristic wavefunction is

$$\psi_{nm}(\boldsymbol{\rho}) = A\exp\left[\mathrm{i}\frac{2\pi}{3L}(2n-m)x\right]\sin\left(\frac{2\pi}{\sqrt{3}L}my\right) - A\exp\left[\mathrm{i}\frac{2\pi}{3L}(2m-n)x\right]\sin\left(\frac{2\pi}{\sqrt{3}L}ny\right) + A\exp\left[-\mathrm{i}\frac{2\pi}{3L}(n+m)x\right]\sin\left[\frac{2\pi}{\sqrt{3}L}(n-m)y\right], \quad (4)$$

and the other is its complex conjugate $\psi^*_{nm}(\boldsymbol{\rho})$ in which n and m are natural numbers. $\psi_{nm}(\boldsymbol{\rho})$ satisfies the relation $\psi_{nm}(\boldsymbol{\rho}) = -\psi_{mn}(\boldsymbol{\rho})$. The normalization constant A is given as $A = (\sqrt{8\sqrt{3}})/(3L)$. The eigenenergy is expressed as $E^{(j)}_{nm} = E_{nm} + E_{zj}$ where

$$E_{nm} = \frac{8\pi^2\hbar^2}{9m^*L^2}(n^2 - mn + m^2). \quad (5)$$

Equations (4) and (5) are the same as those obtained by Krishnamurthy *et al* [11]. Hereafter we label a state (n, m). Because $E^{(j)}_{mn} = E^{(j)}_{nm}$, there exists a duplicate degeneracy in the eigenstates. In addition to this, the present system has another degeneracy between states having different quantum numbers; (1, 3) and (2, 3), (1, 4) and (3, 4), and so forth. It should be noted that $\psi_{nn}(\boldsymbol{\rho})$ is zero anywhere inside the triangle though $E_{nn} \neq 0$. The state $\psi_{nn}(\boldsymbol{\rho})$, therefore, cannot be an eigenstate.

In the case of the InAs (111)A surface, there exist two subbands [9]. To calculate STM images we used the values obtained by Kanisawa *et al* [9]; $E_{z0} = -0.073$ eV and $E_{z1} = -0.0083$ eV. Figure 1 shows energy levels $E^{(0)}_{nm}$ and $E^{(1)}_{nm}$ obtained for a triangular QD whose side length is 48.7 nm. Because E_{nm} is common to both subbands, the sequence of broken lines is the same as that of solid lines, and a sequence of $E^{(1)}_{nm}$ is shifted upward by an amount 64.7 meV with respect to $E^{(0)}_{nm}$. It is obvious that the distribution of $E^{(j)}_{nm}$ is not uniform and becomes dense above 20 meV and then sparse around 100 meV. Hence, STM images observed in the range of bias voltages between 60 and 130 mV are likely to show complex patterns compared with those at lower bias voltages. The numerals in a curly bracket show an electron state (n, m) in which boldfaced numerals represent the states of the subband $z0$ and lightfaced numerals represent the states of the subband $z1$.

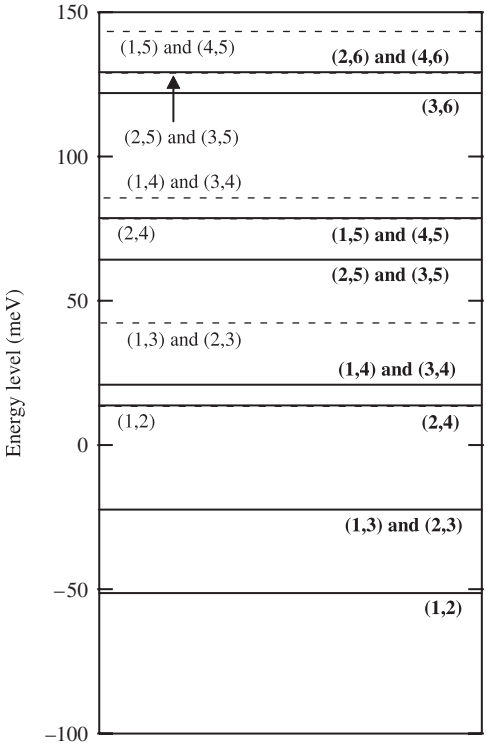

Figure 1. Energy-level diagram of electrons confined in a triangular InAs QD whose side length is 48.7 nm. Solid lines show the sequence of $E_{nm} + E_{z0}$ and broken lines show that of $E_{nm} + E_{z1}$.

3. STM images

On the basis of Bardeen's treatment [12] on the tunneling Hamiltonian, Tersoff and Hamann [13] and Lang [14] obtained the STM current flowing between the apex of an STM tip and a specimen. Selloni *et al* [15] considered the voltage dependence of the STM current which is expressed as follows.

$$I_+(\boldsymbol{\rho}, z(\boldsymbol{\rho}), V) \propto \int_{-\infty}^{+\infty} D(\boldsymbol{\rho}, E)[f_{\mathrm{tip}}(E - eV) - f_{\mathrm{sp}}(E)]T(E - E_{\mathrm{F}}, V, z(\boldsymbol{\rho}))\,\mathrm{d}E, \quad (6)$$

where $f_{\mathrm{tip}}(E)$ and $f_{\mathrm{sp}}(E)$ represent the Fermi distribution function at an absolute temperature T. The factor $[f_{\mathrm{tip}}(E - eV) - f_{\mathrm{sp}}(E)]$ restricts contributions from eigenstates whose energy range is between E_{F} and $E_{\mathrm{F}} + eV$. Because Kanisawa *et al* [9, 10] observed STM images at 5.3 K, Fermi distribution functions can be regarded as step functions. Subscripts 'tip' and 'sp' denote the STM tip and the specimen, respectively. V represents the bias voltage with respect to the Fermi level E_{F}. Because the 2DEG has a narrow band in the order of 100 meV, equation (6) is applicable to the present QD. $D(\boldsymbol{\rho}, E)$ represents the surface local density of states (LDOS), and is expressed in the eigenfunction expansion form as

$$D(\boldsymbol{\rho}, E) = \sum_j \sum_{\sigma nm} w_j |\psi_{nm}(\boldsymbol{\rho})|^2 \times \frac{\Gamma^{(j)}_{nm}}{2\pi\,[(E - E^{(j)}_{nm})^2 + (\frac{1}{2}\Gamma^{(j)}_{nm})^2]}, \quad (7)$$

where $\Gamma^{(j)}_{nm}$ is the energy width associated with the eigenenergy $E^{(j)}_{nm}$. The σ represents spin degrees of freedom. To avoid the increase in fitting parameters, we simply introduce a weighting parameter w_j in the LDOS. As regards the widths of energy levels, we phenomenologically define $\Gamma^{(j)}_{nm} = \Gamma^{\mathrm{QD}(j)}_{nm} + \Gamma_{\mathrm{CS}}$

in which $\Gamma_{nm}^{\mathrm{QD}(j)}$ comes from the electron tunneling through side edges of the QD and Γ_{CS} comes from the lifetime of the electron on a clean surface. The inverse $\hbar/\Gamma_{nm}^{(j)}$ represents the lifetime of the electron remaining in a subband zj.

The transition probability $T(E, V, z(\boldsymbol{\rho}))$ can be written as

$$T(E,V,z(\boldsymbol{\rho})) = \exp\left[-z(\boldsymbol{\rho})\sqrt{(4m^*/\hbar^2)(W_{\mathrm{sp}} + W_{\mathrm{tip}} + eV - 2E)}\right], \quad (8)$$

by WKB approximation where the triangular barrier potential between the surface and an STM tip is approximated as of a square shape. The $z(\boldsymbol{\rho})$ represents the height of the STM tip with respect to the specimen surface. Because the work function of InAs is 5.3 eV and that of the STM tip (tungsten) is 4.55 eV, the term $(eV - 2E)$ in equation (8) is negligible. In this manner we carried out integration over E in equation (6) and obtained the STM current as follows.

$$I_+(\boldsymbol{\rho},z(\boldsymbol{\rho}),V) = K_0 \exp[-\alpha z(\boldsymbol{\rho})] \times \sum_j \sum_{\sigma nm} w_j |\psi_{nm}(\boldsymbol{\rho})|^2 [S_{nm}^{(j)}(V) - S_{nm}^{(j)}(0)], \quad (9)$$

where $S_{nm}^{(j)}(V) = \mathrm{Arctan}[2(E_{\mathrm{F}} + eV - E_{nm}^{(j)})/\Gamma_{nm}^{(j)}]$, $\alpha = \sqrt{(4m^*/\hbar^2)(W_{\mathrm{sp}} + W_{\mathrm{tip}})}$ and K_0 is a constant.

The first derivative of the current with respect to V can be obtained as

$$\frac{\mathrm{d}I_+}{\mathrm{d}V} \propto F(\boldsymbol{\rho}, V) D(\boldsymbol{\rho}, E_{\mathrm{F}} + eV), \quad (10)$$

by assuming that the STM current is nearly constant and neglecting the term $\partial T(E,V,z(\boldsymbol{\rho},V))/\partial V$ which appears in the integrand of equation (6). The function $F(\boldsymbol{\rho},V)$ is defined by the following equation;

$$F(\boldsymbol{\rho},V) = \left\{\sum_j \sum_{\sigma\ nm} w_j |\psi_{nm}(\boldsymbol{\rho})|^2 [S_{nm}^{(j)}(V) - S_{nm}^{(j)}(0)]\right\}^{-1}. \quad (11)$$

The factor $F(\boldsymbol{\rho},V)$ comes from the transition probability $T(E,V,z(\boldsymbol{\rho}))$ through $\exp[-\alpha z(\boldsymbol{\rho})]$ in equation (9). If $T(E,V,z(\boldsymbol{\rho}))$ can be approximated as a constant, $\mathrm{d}I_+/\mathrm{d}V$ corresponds to the LDOS. The $F(\boldsymbol{\rho},V)$ works as the filtering function on the LDOS. Details of these situations are described in our previous article [6]. In reality, the confined electron is subject to tunneling through barrier walls with the increase in energy levels and the energy width increases. Hence we took the energy width as $\Gamma_{nm}^{\mathrm{QD}(j)} = \gamma(E_{nm} + E_{zj})$ where γ is a constant for simplicity.

To obtain $\mathrm{d}I/\mathrm{d}V$ images at bias voltages from +60 to +140 mV, we changed three parameters in the following ranges; the effective mass m^* from 0.035 m_{e} to 0.045 m_{e} in increments of 0.001 m_{e}, the weighting parameter w_0 from 0.50 to 0.95 in increments of 0.05 and a coefficient γ from 0.14 to 0.24 in increments of 0.01. We calculated in total $9 \times 11 \times 11$ patterns of $\mathrm{d}I/\mathrm{d}V$ images for each combination of m^*, w_0 and γ. We obtained the appropriate $\mathrm{d}I/\mathrm{d}V$ image at +100 mV by choosing m^* as $0.039m_{\mathrm{e}}$, and we found that $\mathrm{d}I/\mathrm{d}V$ images are highly sensitive to the value of m^*. The effective mass is 1.7 times greater than the bulk effective mass 0.023 m_{e}.

To pick out the best $\mathrm{d}I/\mathrm{d}V$ image at +80 mV from about 1100 patterns, we set a weighting parameter to be $w_0 = 0.75(w_1 = 0.25)$ and we used this value to calculate $\mathrm{d}I/\mathrm{d}V$ images at other bias voltages. From the feature of probability densities associated with $z0$- and $z1$-states, we can explain the reason why $w_0 > w_1$. The z-component of wavefunction $\phi_1(z)$ has a node in the z-direction, whereas $\phi_0(z)$ has no node. The probability density $|\phi_1(z)|^2$, therefore, has two humps and the hump nearer to the surface is smaller than the other hump far from the surface. Contrary to this, the probability density $|\phi_0(z)|^2$ has a hump higher than those of $|\phi_1(z)|^2$. Hence, we suppose that the electrons occupying a subband state $z0$ make a greater contribution to the $\mathrm{d}I/\mathrm{d}V$ image than those of $z1$-state.

As regards the coefficient γ, we chose $\gamma = 0.2$ to reproduce all experimental $\mathrm{d}I/\mathrm{d}V$ images, and we set the energy width of the clean surface to be equal to $\Gamma_{\mathrm{CS}} = 5$ meV because values greater than 10 meV modify $\mathrm{d}I/\mathrm{d}V$ images.

Through these procedures, we obtained the $\mathrm{d}I/\mathrm{d}V$ images shown in figures 2(a)–(e). Though the $\mathrm{d}I/\mathrm{d}V$ images at +100, +120 and +140 mV are consistent with experimental ones [10], images at +60 and +80 mV are not in good agreement with experimental images in precise detail. There is no bright spot at the center of figure 2(a). At +80 mV the spot at the center has a slightly triangular shape and two peaked fringes exist along a side, whereas three peaked fringes exist in the experimental image.

To resolve these discrepancies, we lowered the energy levels E_{z0} by about 10 meV because the applied voltage enhances the band bending when the number of electrons in the accumulation layer is small and the bias voltage is low [9]. In contrast, when the higher bias voltage is applied to the system, the number of electrons becomes large and the applied electric field is screened by the many body effect of Coulomb interactions [9]. In this case, the applied bias voltages do not affect the energy levels E_{z1}.

Figure 3(a) shows the $\mathrm{d}I/\mathrm{d}V$ image at +60 mV obtained by selecting E_{z0} as −0.087 eV (the energy shift is set at −14 meV), and figure 3(b) shows that at +80 meV obtained by selecting E_{z0} as −0.083 eV (the energy shift is set at −10 meV). The wavefunction associated with the subband z1 has a node in the z-direction and a longer decaying tail toward the bulk than that associated with the subband $z0$. We suppose that the electrons in the subband $z1$ are not as sensitive to the applied bias voltage as compared to the electrons in the subband $z0$. Hence we neglected the energy shift of E_{z1}. Images in figures 3(a) and (b) are consistent with experimental ones yielding a spot at the center in figure 3(a) and three fringes near a side in figure 3(b). We found that the center spot of both images is made of (1, 5)- and (4, 5)-states. It should be noted that the reduction in E_{z0} is necessary for deriving $\mathrm{d}I/\mathrm{d}V$ images of the present system.

To demonstrate an example of introducing weighting parameters w_0 and w_1, we show $\mathrm{d}I/\mathrm{d}V$ images including only electron states of a subband $z0$ and only those of a subband $z1$ in figures 4(a) and (b), respectively. It is obvious that the image in figure 3(b) is quite different from figures 4(a) and (b).

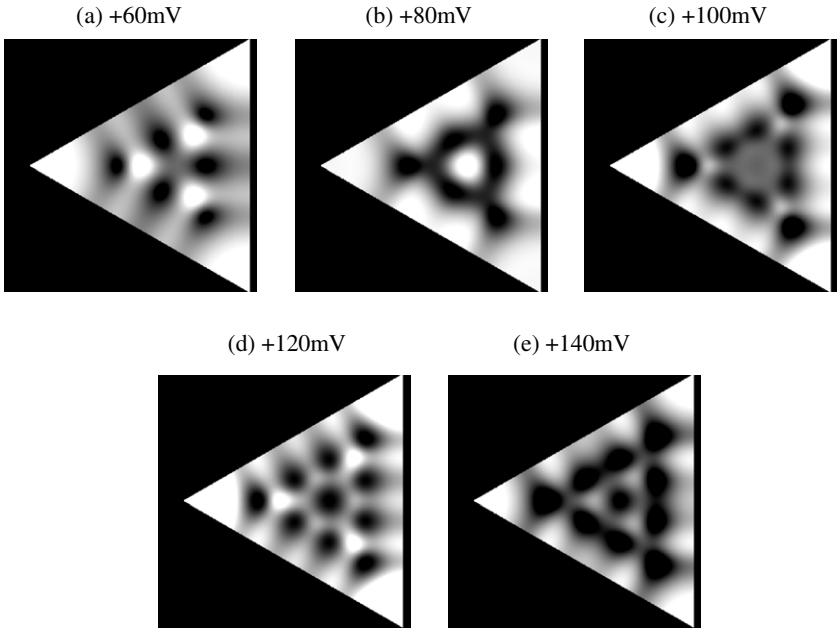

Figure 2. $\mathrm{d}I/\mathrm{d}V$ images obtained by considering contributions from both subbands; $z0$ and $z1$. The side length is 48.7 nm.

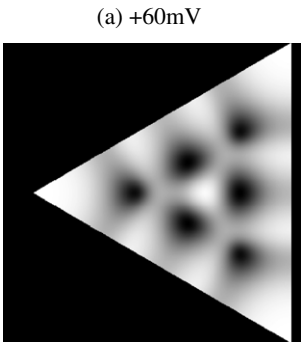

Figure 3. $\mathrm{d}I/\mathrm{d}V$ images obtained by setting (a) $E_{z0} = -0.083$ eV and (b) $E_{z0} = -0.087$ eV. The side length is 48.7 nm. Weighting parameters were set at $w_0 = 0.75$ and $w_1 = 0.25$.

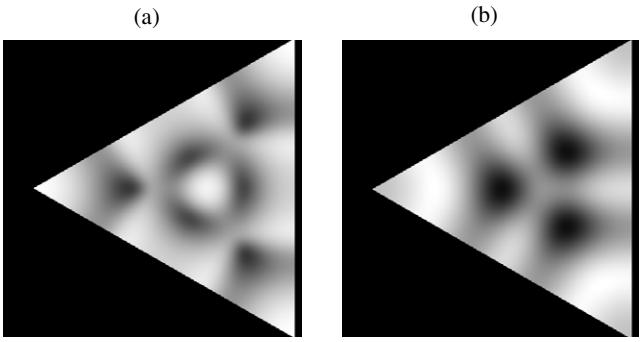

Figure 4. $\mathrm{d}I/\mathrm{d}V$ image at +80 mV; (a) contributions from only a subband $z0$ are considered, and (b) contributions from only a subband $z1$ are considered. The side length is 48.7 nm.

We found that dark areas surrounding each center are rotated by 60°. Hence the combination of both images yields a larger dark area surrounding the center spot in figure 3(b). Obviously twin peaked fringes near a side in figure 4(a) and one peaked fringe near a side in figure 4(b) combine into a three peaked fringe in figure 3(b).

Figures 5(a)–(d) show the effect of the filtering function $F(\boldsymbol{\rho}, V)$ on the LDOS image for the triangular QD whose side length is 48.7 nm; the intensity product of figures 5(a) and (b) yields figure 3(a), and the product of figures 5(c) and (d) yields figure 2(e). We should note that LDOS images are shrunk because the wavefunctions are zero at triangle boundaries. It is obvious that connected spots near three sides of figures 5(b) and (d) are extended to three rims of the triangle as are shown in figures 3(a) and 2(e). The reason for this is that both a numerator and a denominator in equation (10) have the same factor $|\psi_{nm}(\boldsymbol{\rho})|^2$, which makes the limiting value of $\mathrm{d}I/\mathrm{d}V$ finite on three sides.

Figure 6 shows our $\mathrm{d}I/\mathrm{d}V$ images for the QD whose side length is 33.9 nm. The intensity at three sides is finite in contrast to LDOS images shown in figures 5(b) and (d). At +100 mV there exists a sharp peak at the center, whereas the image calculated by Kanisawa *et al* [10] has no peak at the center. As regards our $\mathrm{d}I/\mathrm{d}V$ image at +120 mV, there exists a hump of high intensity at each mid position of three sides and a hump at each corner. In addition there is no spot at the center. These features are common to experimental images. Hence we found that our 3D images reproduce the experimental images well. In contrast to our results, the images calculated by Kanisawa *et al* [10] show the intensity imbalance at distributed humps; the intensity at three corners is much lower than that of the experimental images. Moreover, although the experimental $\mathrm{d}I/\mathrm{d}V$ images show a finite intensity at three sides, their calculated images show a much lower intensity there.

Here we reproduce LDOS images obtained by Kanisawa *et al* [10] from our point of view. Figure 7 shows probability

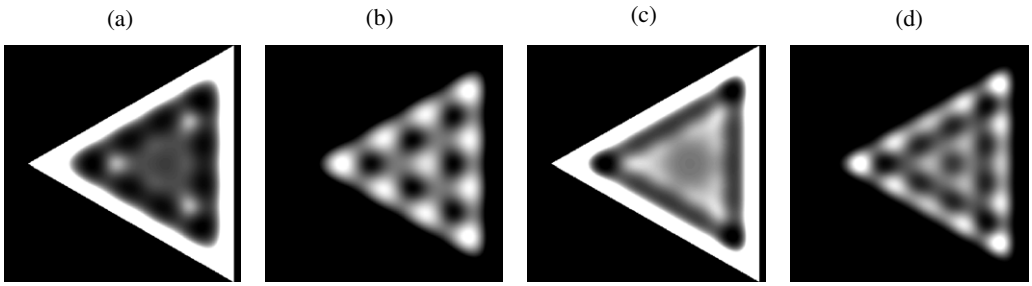

Figure 5. (a) Image of $F(\boldsymbol{\rho}, V)$ and (b) LDOS image obtained at +60 mV, and (c) image of $F(\boldsymbol{\rho}, V)$ and (d) LDOS image obtained at +140 mV.

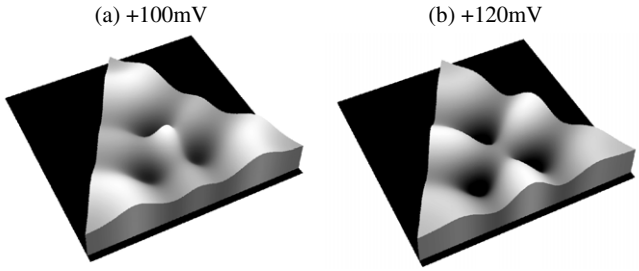

Figure 6. 3D patterns of $\mathrm{d}I/\mathrm{d}V$ images for a triangular QD whose side length is 33.9 nm.

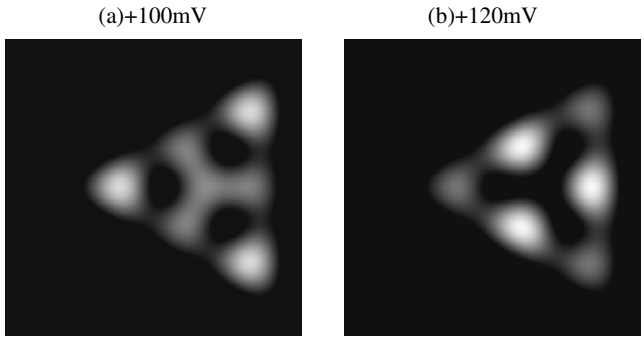

Figure 7. Probability densities of a triangular QD whose side length is 33.9 nm. (a) superposed probability density $[|\psi_{14}(\boldsymbol{\rho})|^2 + |\psi_{24}(\boldsymbol{\rho})|^2]/2$, and (b) $|\psi_{14}(\boldsymbol{\rho})|^2$.

densities of electrons confined in a triangular QD having a side length 33.9 nm long. By using the wave functions shown in equation (4), we made linear combinations of probability densities; $[|\psi_{14}(\boldsymbol{\rho})|^2 + |\psi_{24}(\boldsymbol{\rho})|^2]/2$, and the probability density $|\psi_{14}(\boldsymbol{\rho})|^2$ where $E_{z0} = -0.073$ eV. Though these images are in good agreement with those calculated by Kanisawa *et al* [10], they are not consistent with experimental images as shown above. In this manner, a simple combination of probability densities is not applicable to the analysis of STM images.

Kanisawa *et al* [10] calculated LDOS images for the triangular QD having a side length 17.3 nm. Though we calculated the $\mathrm{d}I/\mathrm{d}V$ image at +80 mV for the QD whose side length is 17.3 nm, we could not obtain an image consistent with the experimental one. Figure 8 shows our result. The reason for this inconsistency is the short side length of the QD and

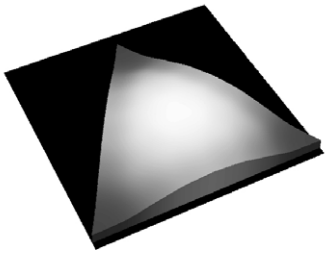

Figure 8. 3D pattern of the $\mathrm{d}I/\mathrm{d}V$ image at +80 mV. The side length is 17.3 nm.

its resultant distribution of energy levels. The image is mainly composed of the (1, 2)-state which gives only a single hump at the center. The energy level of the (1, 2)-state is estimated as $E_{12} + E_{z0} = +83$ meV. Because $E_{13} + E_{z0} = E_{23} + E_{z0} = +290$ meV, the $\mathrm{d}I/\mathrm{d}V$ image is insensitive to bias voltages ranging from +80 to +160 mV. Therefore, we changed the side length 17.3 nm to 27.3 nm which gives proper $\mathrm{d}I/\mathrm{d}V$ images.

Figure 9 shows the $\mathrm{d}I/\mathrm{d}V$ images calculated by equation (10) for the triangular QD whose side length is 27.3 nm. In contrast to figure 8, these images have three humps, which is consistent with experimental ones. The peak positions of these $\mathrm{d}I/\mathrm{d}V$ images are almost the same at different bias voltages. It should be noted that these images have finite intensities at three sides, which can be seen by experimental images displayed with a density-plotting [16] but cannot be identified well by the 3D images shown in [10].

We may claim that STM images calculated by Kanisawa *et al* [10] are different from experimental $\mathrm{d}I/\mathrm{d}V$ images. Since they did not show the explicit expression of LDOS, we cannot evaluate STM images calculated by them. We suppose that they related probability densities to LDOS calculated by using some tight-binding method. Hence, it is likely that their LDOS images have zero intensity at triangle boundaries, which is a feature common to their LDOS images.

To explain another $\mathrm{d}I/\mathrm{d}V$ image observed by Kanisawa *et al* (figure 1(b) of [17]), we calculated the image observable at a bias voltage +300 mV for the InAs QD whose side length is 28 nm. Figure 10 shows our result by setting the effective mass to be $m^* = 0.050\ m_\mathrm{e}$ which is about twice the effective mass $0.023\ m_\mathrm{e}$ of the bulk InAs. This enhancement indicates that energy levels in the high energy range are lowered compared to those estimated by using an effective mass $0.039 m_\mathrm{e}$. Our

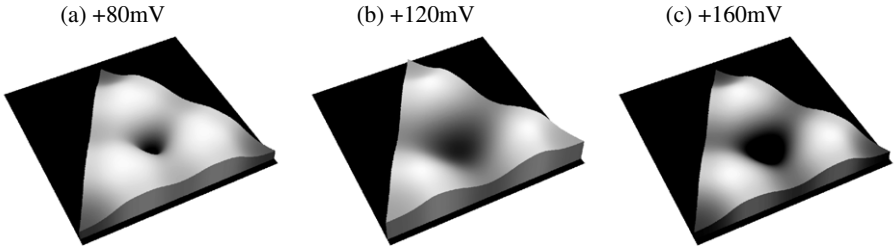

Figure 9. 3D patterns of $\mathrm{d}I/\mathrm{d}V$ images at three bias voltages. The side length is 27.3 nm.

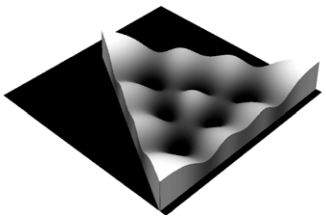

Figure 10. 3D pattern of the $\mathrm{d}I/\mathrm{d}V$ image for a triangular QD whose side length is 28 nm. The bias voltage is set at +300 mV.

image is consistent with the experimental one; a spot at the center and two humps along three sides.

4. Conclusion

We showed that experimental STM images for the electrons confined in the equilateral triangular quantum dot of InAs (111)A surface can be explained by the eigenstates and the eigenenergies obtained by the one-particle model presented here. Hence we can regard triangle edges as potential barriers for a confined electron.

We showed that the $\mathrm{d}I/\mathrm{d}V$ image is not the LDOS image; the intensity of $\mathrm{d}I/\mathrm{d}V$ image at triangle boundaries is finite, whereas the intensity of LDOS image is very small there. It is impossible to explain $\mathrm{d}I/\mathrm{d}V$ images by LDOS images or by images of probability densities of confined electrons. Our expressions for the $\mathrm{d}I/\mathrm{d}V$ and the LDOS are shown to be applicable to both metallic QCs and semiconductor QDs.

We clarified that contributions from the electrons occupying two subbands are decisive in explaining experimental $\mathrm{d}I/\mathrm{d}V$ images, and the lowering of the subband energy level induced by an applied bias voltage is necessary for analyzing STM images especially at low bias voltages. We found that the energy level of a subband E_{z0} is shifted downward by -14 meV at the bias voltage +60 mV and by -10 meV at the bias voltage +80 mV. We also found that the effective mass of 2DEG is 0.039 m_e in the energy range from +60 to +160 meV. At +300 meV, the effective mass is found to be 0.050 m_e.

References

[1] Crommie M F, Lutz C P and Eigler D M 1993 *Science* **262** 218
[2] Crommie M F, Lutz C P, Eigler D M and Heller J 1995 *Physica* D **83** 98
[3] Fiete G A and Heller E J 2003 *Rev. Mod. Phys.* **75** 933 and references therein
[4] Diekhöner L, Schneider M A, Baranov A N, Stepanyuk V S, Bruno P and Kern K 2003 *Phys. Rev. Lett.* **90** 236801
[5] Kevan S D and Gaylord R H 1987 *Phys. Rev.* B **36** 5809
[6] Kumagai T and Tamura A 2008 *J. Phys. Soc. Japan* **77** 014601
[7] Rieder K H, Meyer G, Braun K F, Hla S W, Moresco F, Morgenstern K, Repp J, Foelsch S and Bartels L 2003 *Europhys. News* **34** 95
[8] Kouwenhoven F, Austing D G and Tarucha A 2001 *Rep. Prog. Phys.* **64** 701 and references therein
[9] Kanisawa K, Butcher M J, Yamaguchi H and Hirayama Y 2001 *Phys. Rev. Lett.* **86** 3384
[10] Kanisawa K, Butcher M J, Tokura Y, Yamaguchi H and Hirayama Y 2001 *Phys. Rev. Lett.* **87** 196804
[11] Krishnamurthy H R, Mani H S and Verma H C 1982 *J. Physique* A **15** 2131
[12] Bardeen J 1961 *Phys. Rev. Lett.* **6** 57
[13] Tersoff J and Hamann D R 1983 *Phys. Rev. Lett.* **50** 1998
Tersoff J and Hamann D R 1985 *Phys. Rev.* B **31** 805
[14] Lang N D 1985 *Phys. Rev. Lett.* **55** 230
Lang N D 1985 *Phys. Rev.* B **34** 5947
[15] Selloni A, Carnevali P, Tosatti E and Chen C D 1985 *Phys. Rev.* B **31** 2602
[16] Kanisawa K, Tokura Y, Yamaguchi H and Hirayama Y 2002 *Research 2002 Activities in NTT Basic Research Laboratories* vol 12, p 23 http://www.brl.ntt.co.jp/E/activities/file/report01/BRLReport12_E.pdf
[17] Kanisawa K, Tokura Y, Yamaguchi H and Hirayama Y 2005 *Proc. 27th Int. Conf. on the Physics of Semiconductors* ed J Menédez and C G Van de Walle (New York: AIP) p 825